Reduction of aryl halides by consecutive visible light-induced electron transfer processes

Indrajit Ghosh *et al.*

Science **346**, 725 (2014);
DOI: 10.1126/science.1258232

At the boundary between two topologically distinct segments of edge, localized exotic topological zero modes arise that give rise to topologically protected degeneracies and projective non-Abelian statistics (*12*). In the case of the Z_2 sRVB state, the domain wall between e and m edges localizes a Majorana fermion zero mode, with the following physical consequences: Let us consider the case of the superconductivity-induced e edge, where an electron can coherently enter the QSL as a fermionic spinon. If this process occurs in the vicinity of the domain wall between an e and m edge, then the fermionic spinon can also emit or absorb a vison from the m edge, thus becoming a bosonic spinon. In other words, the Majorana fermion zero mode is a source or sink of fermion parity, allowing the electron to coherently enter into the spin liquid as a bosonic spinon. If the fermionic spinon in the bulk of the QSL can decay into a vison and a bosonic spinon, then this geometry (Fig. 1B) will allow the Tomasch oscillations to be observed in the tunneling conductance. Similar considerations show that when the e edge is induced by magnetism, the electron can enter into the spin liquid as a bosonic holon in the vicinity of the e-m domain wall (Fig. 1D).

The considerations outlined here suggest ways to tune through the topological phase transition that separates the e and m edges, such as by applying a magnetic field to the edge of an easy-plane QSL. This can be done by taking a thin sample and shielding the bulk of the QSL by sandwiching it between two superconductors. At the critical field for the edge quantum phase transition, there will be enhanced thermal transport through the edge, leading to a nonzero intercept at low temperatures in the thermal conductance: $\lim_{T\to 0}\kappa/T = N_{\mathrm{L}} c \frac{\pi^2}{3}\frac{k_{\mathrm{B}}^2}{h}$, where N_{L} is the number of layers in the QSL, $c = 1/2$ is the central charge of the edge at the critical point, and k_{B} is Boltzmann's constant. Because neither the trivial paramagnet nor the doubled-semion QSL have topologically distinct types of gapped boundaries, the observation of a topological quantum phase transition at the edge of a gapped insulating spin system would prove the existence of a fractionalized spin-liquid state and rule out the doubled-semion state. The present considerations are readily extended to other sorts of topologically ordered states, such as those that occur in fractional quantum Hall systems.

REFERENCES AND NOTES

1. P. W. Anderson, *Mater. Res. Bull.* **8**, 153–160 (1973).
2. S. A. Kivelson, D. S. Rokhsar, J. P. Sethna, *Phys. Rev. B* **35**, 8865–8868 (1987).
3. N. Read, S. Sachdev, *Phys. Rev. Lett.* **66**, 1773–1776 (1991).
4. X. G. Wen, *Phys. Rev. B* **44**, 2664–2672 (1991).
5. T. Senthil, M. P. A. Fisher, *Phys. Rev. B* **62**, 7850–7881 (2000).
6. R. Moessner, S. L. Sondhi, *Phys. Rev. Lett.* **86**, 1881–1884 (2001).
7. L. Balents, M. P. A. Fisher, S. M. Girvin, *Phys. Rev. B* **65**, 224412 (2002).
8. A. Seidel, *Phys. Rev. B* **80**, 165131 (2009).
9. L. Balents, *Nature* **464**, 199–208 (2010).
10. M. Barkeshli, X.-L. Qi, *Phys. Rev. X* **2**, 031013 (2012).
11. M. Barkeshli, C.-M. Jian, X.-L. Qi, *Phys. Rev. B* **87**, 045130 (2013).
12. M. Barkeshli, C.-M. Jian, X.-L. Qi, *Phys. Rev. B* **88**, 241103(R) (2013).
13. S. Beigi, P. W. Shor, D. Whalen, *Commun. Math. Phys.* **306**, 663–694 (2011).
14. A. Kitaev, L. Kong, *Commun. Math. Phys.* **313**, 351–373 (2012).
15. M. Levin, *Phys. Rev. X* **3**, 021009 (2013).
16. A. Kapustin, N. Saulina, *Nucl. Phys. B* **845**, 393–435 (2011).
17. N. H. Lindner, E. Berg, G. Refael, A. Stern, *Phys. Rev. X* **2**, 041002 (2012).
18. D. J. Clarke, J. Alicea, K. Shtengel, *Nat. Commun.* **4**, 1348 (2013).
19. M. Cheng, *Phys. Rev. B* **86**, 195126 (2012).
20. M. Punk, D. Chowdhury, S. Sachdev, *Nat. Phys.* **10**, 289–293 (2014).
21. T.-H. Han *et al.*, *Nature* **492**, 406–410 (2012).
22. Y. Qi, C. Xu, S. Sachdev, *Phys. Rev. Lett.* **102**, 176401 (2009).
23. These were identified long ago in the toric code model (*38*) in terms of rough versus smooth edges (*39*), although the generic necessity to realize one or the other in resonating valence bond states and their general independence of lattice structure has only recently been fully appreciated.
24. D. S. Rokhsar, S. A. Kivelson, *Phys. Rev. Lett.* **61**, 2376–2379 (1988).
25. T. Senthil, O. Motrunich, *Phys. Rev. B* **66**, 205104 (2002).
26. M. Freedman, C. Nayak, K. Shtengel, K. Walker, Z. Wang, *Ann. Phys.* **310**, 428–492 (2004).
27. X.-G. Wen, *Quantum Field Theory of Many-Body Systems* (Oxford Univ. Press, Oxford, 2004).
28. H.-C. Jiang, Z. Wang, L. Balents, *Nat. Phys.* **8**, 902–905 (2012).
29. H.-C. Jiang, H. Yao, L. Balents, *Phys. Rev. B* **86**, 024424 (2012).
30. S. Yan, D. A. Huse, S. R. White, *Science* **332**, 1173–1176 (2011).
31. S. Depenbrock, I. P. McCulloch, U. Schollwöck, *Phys. Rev. Lett.* **109**, 067201 (2012).
32. See the supplementary materials on *Science* Online.
33. If the resulting gaps are large, the field theory description of the edge is no longer controlled, but because the most important qualitative features of a gapped state do not depend on the magnitude of the gap, the field theory description of such phases should be adequate for present purposes: More formally, it gives a leading order description of the edge modes in the vicinity of an edge quantum critical point where the edge gaps, but not the bulk gaps, are vanishingly small.
34. W. J. Tomasch, *Phys. Rev. Lett.* **15**, 672–675 (1965).
35. W. L. McMillan, P. W. Anderson, *Phys. Rev. Lett.* **16**, 85–87 (1966).
36. S. Kivelson, D. Rokhsar, *Phys. Rev. B* **41**, 11693–11696 (1990).
37. M. Barkeshli, H. Yao, S. A. Kivelson, *Phys. Rev. B* **87**, 140402 (2013).
38. A. Kitaev, *Ann. Phys.* **303**, 2–30 (2003).
39. S. B. Bravyi, A. Y. Kitaev, http://arxiv.org/abs/quant-ph/9811052.

ACKNOWLEDGMENTS

This work was supported by NSF-DMR grant 1265593 (S.K.), the Israel Science Foundation, the Israel-U.S. Binational Foundation, the Minerva Foundation, and the German-Israeli Foundation (E.B.). M.B. thanks X.-L. Qi for recent collaborations on related topics. We thank E. Altman, C. Nayak, M. Freedman, Z. Wang, K. Walker, M. Hastings, M. P. A. Fisher, B. Bauer, and T. Grover for discussions.

SUPPLEMENTARY MATERIALS

www.sciencemag.org/content/346/6210/722/suppl/DC1
Supplementary Text
References (*40*–*45*)

12 March 2014; accepted 2 October 2014
10.1126/science.1253251

PHOTOCHEMISTRY

Reduction of aryl halides by consecutive visible light-induced electron transfer processes

Indrajit Ghosh,* Tamal Ghosh,* Javier I. Bardagi, Burkhard König†

Biological photosynthesis uses the energy of several visible light photons for the challenging oxidation of water, whereas chemical photocatalysis typically involves only single-photon excitation. Perylene bisimide is reduced by visible light photoinduced electron transfer (PET) to its stable and colored radical anion. We report here that subsequent excitation of the radical anion accumulates sufficient energy for the reduction of stable aryl chlorides giving aryl radicals, which were trapped by hydrogen atom donors or used in carbon-carbon bond formation. This consecutive PET (conPET) overcomes the current energetic limitation of visible light photoredox catalysis and allows the photocatalytic conversion of less reactive chemical bonds in organic synthesis.

Visible light provides sufficient energy to promote challenging chemical reactions. Biological photosynthesis as the omnipresent example uses a visible portion of the solar spectrum to separate charges by electron transfer, providing the energy for water oxidation. This transformation (water to oxygen, protons, and electrons) requires the cumulative absorption of four photons (*1*). In past decades, visible light–mediated chemical photoredox catalysis has emerged into a conceptually related valuable method for organic synthesis (*2*–*4*). Here, single-photon excitation of dye molecules, such as redox-active coordination compounds [e.g., $Ru(bpy)_3^{2+}$ or $Ir(ppy)_3$] (*3*, *5*), conjugated organics (e.g., eosin Y) (*6*), or inorganic semiconductors (e.g., CdS) (*7*) mediates photoinduced electron or energy transfer process to substrates.

A recent application is the generation of highly reactive aryl radicals, which are useful arylating reagents in synthesis, by photoinduced electron transfer (PET) from photoredox catalysts to suitable precursors followed by bond scission (*8*, *9*). However, the choice of aryl radical precursors is currently limited to electron-poor arenes, such as diazonium (*6*, *10*) or iodonium (*11*) salts, or in a few cases aryl iodides (*9*, *12*), with weakly bound leaving groups, due to the accessible reducing

Institute of Organic Chemistry, University of Regensburg, D-93040 Regensburg, Germany.
*These authors contributed equally to this work. **†Corresponding author. E-mail: burkhard.koenig@ur.de**

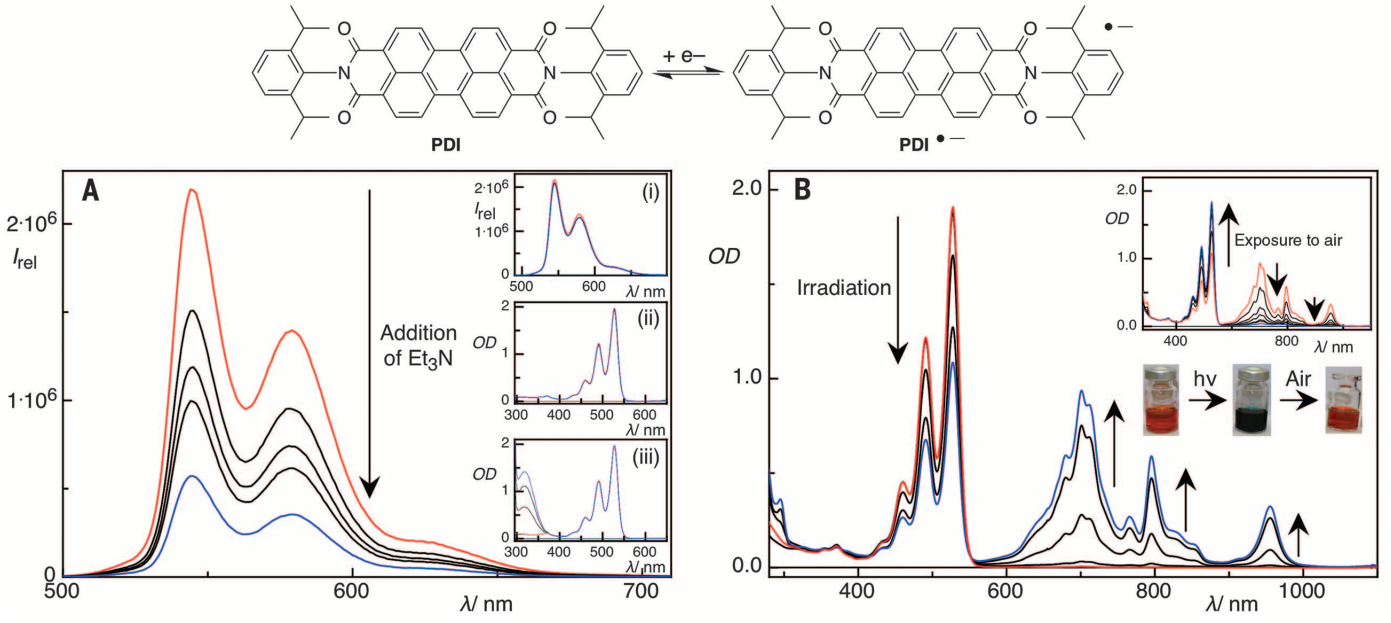

Fig. 1. Chemical structure of the photocatalyst PDI, one electron reduction of PDI to its radical anion, and effects of Et_3N and 4′-bromoacetophenone on its photophysical properties. (**A**) Changes in the fluorescence spectra (in this case, intensity; λ_{Ex} = 455 nm) of PDI upon successive addition of Et_3N in DMF. In the insets, changes in the fluorescence spectra of PDI upon addition of (i) 4′-bromoacetophenone, and changes in the absorption spectra of PDI upon addition of (ii) Et_3N, and (iii) 4′-bromoacetophenone are shown. (**B**) Formation of the PDI radical anion ($PDI^{\bullet-}$) upon photoexcitation (λ_{Ex} = 455 nm) of PDI in the presence of Et_3N. In the inset, regeneration of neutral PDI from $PDI^{\bullet-}$ upon exposure to air is shown (see also fig. S5).

power of typical visible light photoredox catalysts (*13*, *14*). Two mechanistic scenarios for the aryl radical generation can be considered: (i) oxidative quenching of the excited photoredox catalyst by the aryl radical precursor, which must be exergonic or, if the lifetime of the excited state is long and the subsequent bond cleavage fast and irreversible, at least thermo neutral (*15*); (ii) oxidation of the photoreduced catalyst in its ground state (fig. S1, left), which can be slightly endergonic. The energy conferred by visible light excitation for subsequent reduction chemistry is limited by the energy of a single absorbed photon. The energy of blue photons (440 nm) of 270 KJ/mol or 2.8 eV defines a maximum theoretical energy threshold between the donor (i.e., photocatalyst) and acceptor (i.e., substrate). In addition, part of the accessible energy is always lost due to intersystem crossing and reorganization of the excited states of the photocatalysts by nonradiative pathways. In the case of Ru complexes, this loss is ~0.6 eV (*3*). As a consequence, the available energy of typical photocatalysts just reaches the reduction potential (E^o) of aryl iodides (*9*), defining the current synthetic scope of photoredox catalysis.

Here, we report a practical approach to overcome the limitations of visible light–mediated chemical photocatalysis by using the energies of two photons in one catalytic cycle (*16*). Photocatalytic alkylation or arylation reactions as reported by MacMillan (*3*, *17*), Stephenson (*18*), Yoon (*2*), and others (*6*) employ a typical PET process (fig. S1, left). The excited dye becomes a stronger oxidant (and reductant) and is converted into its radical anion, which activates substituted benzyl

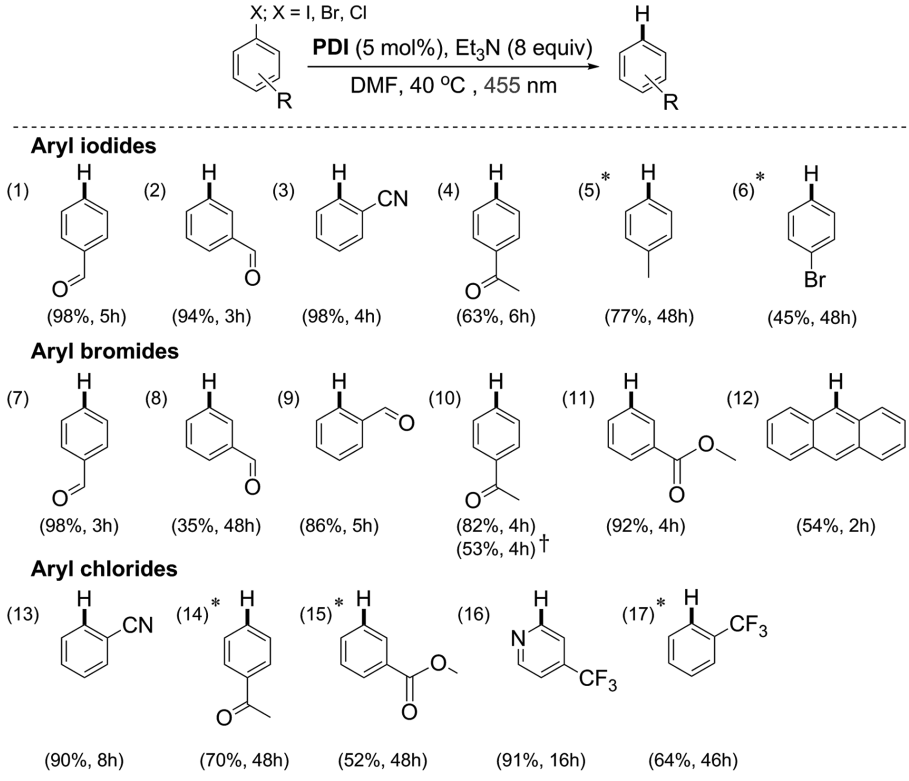

Yields (Error ca. 5 %) were calculated from GC measurements using internal standards.
*10 mol% catalyst and 16 equiv of Et_3N were employed.
†Photoreduction reaction was performed under sunlight.

Fig. 2. Photoreduction of aryl halides. Yields (%) and reaction times (hours) are given.

bromides (*3*, *19*), alpha bromo carbonyl compounds (*20*), aryl iodides (*9*, *12*), diazonium (*6*), and iodonium (*11*) salts. However, compounds that are less reactive (e.g., aryl bromides and chlorides) (*21*–*23*) due to a more negative reduction potential, higher carbon-halide bond dissociation energy, and a different, stepwise cleavage mechanism (*23*) are not accessible by this process using typical photocatalysts and, more importantly, visible light. Our approach is inspired by the Z scheme of biological photosynthesis, which has already been used in water photooxidation (*24*) but, surprisingly, has not yet been applied in organic synthesis. The energy of a second visible light excitation can be added to the process if the radical anion of the dye is reasonably stable in the ground state, colored, and thus can be excited again by visible light (fig. S1, right).

Perylene diimides—a class of fluorescent dye molecules that have been used as pigments, colorants, photoreceptors, and, more recently, as electronic materials because of their characteristic combination of thermal- and photostability and optical and redox properties (*25*)—fulfill the requirements of such a biomimetic organic dye–based catalytic system. Among different perylene diimides *N*,*N*-bis(2,6-diisopropylphenyl)perylene-3,4,9,10-bis(dicarboximide) (PDI) (see Fig. 1 for chemical structure) was selected due to its better solubility in *N*,*N*′-dimethylformamide (DMF) and dimethyl sulfoxide (DMSO) (solvents used in this study). Upon irradiation with blue light (455 nm) in the presence of triethylamine (Et_3N) as electron donor, PDI forms a colored radical anion $PDI^{\bullet-}$ (Fig. 1 and figs. S3 to S5) that can again be excited by visible light (*26*). In the absence of oxygen, the radical anion is very stable. Spectroscopic investigations confirmed that electron transfer from Et_3N to PDI requires photoexcitation (Fig. 1 and fig. S4) (*27*).

A synthetic application of this catalytic system is the photoreduction of aryl halides, including aryl chlorides, using visible light irradiation. The reaction conditions were optimized by irradiating a mixture of 4′-bromoacetophenone, PDI (5 mol%), and Et_3N with blue light (455 nm) (see table S1). In DMSO as solvent, the reduction product acetophenone was obtained in 4 hours with 47% photoreduction yield (entry 16, table S1). Continuous irradiation of the reaction mixture for 8 hours gave 69% yield. Use of DMF as solvent gave comparable or slightly better yields (see entry 10 in Fig. 2 and table S1) in a shorter reaction time of 4 hours. Control experiments confirmed that PDI, electron donor, and light irradiation are necessary for the photoreduction reaction to occur (entries 1 to 6 in table S1).

Using the optimized conditions, the reaction scope was explored with a range of substituted aryl bromides giving the corresponding reduction products in good to nearly quantitative yields (Fig. 2). The reduction potentials of NMe_2- and OMe-substituted aryl bromides are too high to be reached employing these photoreduction conditions, whereas *p*-nitro-substituted aryl bromides have such a low fragmentation rate (*22*) that back electron transfer becomes dominant. The photoreduction reactions could also be performed under sunlight (entry 10 in Fig. 2) or with 530-nm light-emitting diodes as the absorption spectrum of PDI spans a broad portion of the visible spectrum (fig. S3). Substituted aryl iodides having slightly lower reduction potentials than aryl bromides (*22*) gave comparable photoreduction yields (see entries 1 to 6 in Fig. 2). Notably, an aryl–iodine bond was chemoselectively reduced in the presence of a bromine substituent (entry 6 in Fig. 2).

A commercially available catalyst, *N*,*N*′-bis (3-pentyl)perylene-3,4,9,10-bis(dicarboximide) (for the chemical structure, see fig. S2), gave similar yields when the reaction mixtures were irradiated for 8 hours (see entries 14 and 15 in table S1). The slightly slower reaction rate is attributed to its poorer solubility.

Based on the reduction potential of $PDI/PDI^{\bullet-}$ [–0.37 V versus saturated calomel electrode (SCE)] and the $E_{0\text{–}0}$ transition energy of $PDI^{\bullet-}$, we estimated a reducing power of the excited state $PDI^{\bullet-*}$ according to the Rehm-Weller equation (*28*) that reaches or exceeds the reduction potentials of substituted aryl chlorides (*26*, *29*). This class of compounds, although easily accessible and relatively inexpensive, has not been considered in visible light photocatalysis because of their low reactivity due to high reduction potentials, high carbon-chlorine bond energies, and a stepwise fragmentation mechanism. To the best of our knowledge, the reduction of aryl chlorides has only been achieved using strong bases (*30*, *31*), such as potassium tert-butoxide, or nucleophiles under ultraviolet (UV) ($\lambda_{Ex} \leq$ 350 nm) irradiation ($S_{RN}1$) (*32*) and in the presence of an excess of highly reactive neutral organic reducing agents, such as N^2,N^2,N^{12},N^{12}-tetramethyl-7,8-dihydro-6H-dipyrido[1,4]diazepine-2,12-diamine (for the chemical structure, see fig. S2) and UV-A (365 nm) irradiation as introduced by Murphy (*21*). The consecutive PET (conPET) process generates the strong reducing $PDI^{\bullet-*}$ in situ by two subsequent visible light excitations starting from air-stable PDI. This avoids the use of highly air- and

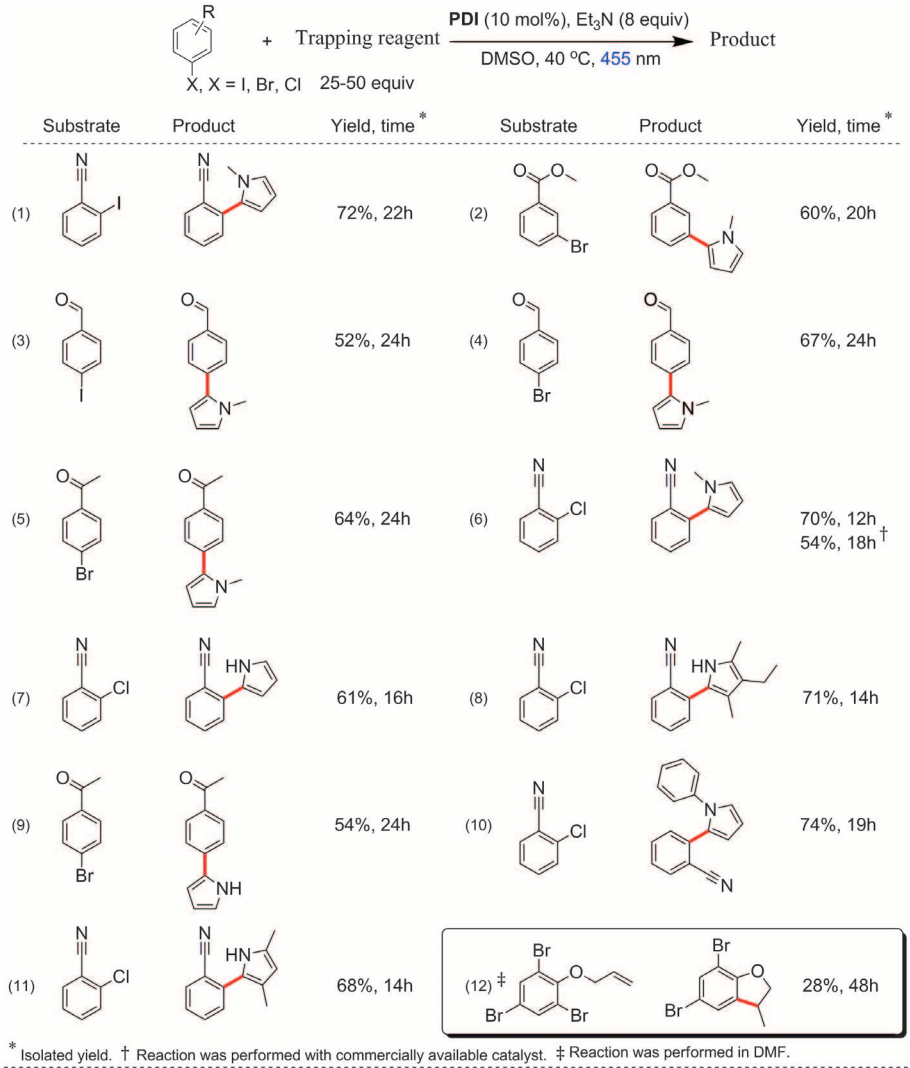

* Isolated yield. † Reaction was performed with commercially available catalyst. ‡ Reaction was performed in DMF.

Fig. 3. C–H aromatic substitution reactions of aryl halides with substituted pyrroles and intramolecular addition to an alkene.

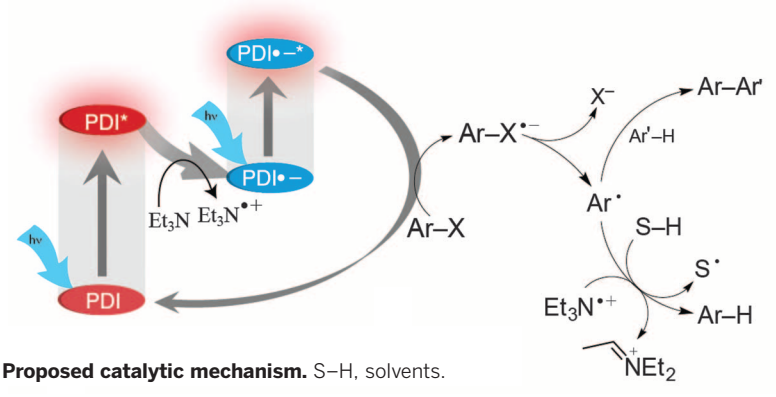

Fig. 4. Proposed catalytic mechanism. S–H, solvents.

moisture-sensitive donor molecules, which require strict inert reaction conditions, UV-A irradiation, and strongly basic conditions that are incompatible with many functional groups. Aryl chlorides bearing electron withdrawing groups gave the corresponding reduction products with good to excellent yields in photocatalytic conditions (entries 13 to 17 in Fig. 2) that require only mixing of substrates, PDI, Et_3N, and irradiation with visible light.

Next, we applied the aryl radical intermediates for C–C bond-forming arylation reactions. Challenge in this case is competition from fast hydrogen abstraction of the aryl radical from the solvent and the radical cation of Et_3N (*33*). We therefore selected as the reaction partner *N*-heterocyclic pyrroles, which were found to have high reaction rates in the addition of radicals. Substantial amounts of the expected arylation product were indeed obtained by irradiating aryl halides in the presence of *N*-methylpyrrole and catalytic amounts of PDI. The reduction product is a minor by-product but dominates when furan or thiophene are used as reaction partner. Changing the solvent from DMF, which favors the reduction product, to DMSO improved the yields greatly. Isolated yields of functionalized *N*-methylpyrrole derivatives obtained from different substituted aryl halides are depicted in Fig. 3. As in the photoreduction reaction, the C–H arylation reaction with *N*-methylpyrrole could also be performed with *N,N'*-bis(3-pentyl)perylene-3,4,9,10-bis(dicarboximide) (entry 6 in Fig. 3). The reaction scope was extended to other pyrrole derivatives affording arylated products in good to excellent yields (Fig. 3).

The photoreduction of aryl halides appears to proceed via a radical mechanism (*23*, *34*), as evidenced by the conversion of 2-(allyloxy)-1,3,5-tribromobenzene to the 5-*exo* cyclization product 5,7-dibromo-3-methyl-2,3-dihydrobenzofuran (entry 12, Fig. 3), which implies a radical intermediate (*12*, *34*). Furthermore, the reduction reaction of 4′-bromoacetophenone in the presence of 2,2,6,6-tetramethylpiperidinoxyl (TEMPO) gave the expected TEMPO adduct (see the supplementary materials). The formation of a PDI dianion, which could be formed via a two-electron reduction (*35*), was not detected under the reaction conditions (compare Fig. 1B and fig. S4 with fig. S3; fig. S3 shows the absorption spectrum of the electrochemically generated PDI dianion). The photoreduction of 4′-bromoacetophenone was minimal in air, preventing the formation of the PDI radical anion (entry 6 in table S1, Fig. 1B, and fig. S5). In the absence of light, no reduction product is obtained: 4′-bromoacetophenone added to a photochemically generated PDI radical anion (by photo-irradiating the mixture of PDI and Et_3N) and kept in the dark for 4 hours was not converted (entries 9 and 11 in table S1). When the reaction mixture was then illuminated with 455-nm light, acetophenone was obtained in yields comparable to the normal photoreduction protocol. Reduction of 4′-bromoacetophenone also did not occur when the substrate was added to a chemically generated [using $(Et_4N)_2S_2O_4$ as chemical reductant of PDI] radical anion (see entry 10 in table S1). Degradation products of the catalyst formed during the course of the reaction may still contribute to substrate conversion because only the perylene core is required (compare PDI and *N,N'*-bis(3-pentyl)perylene-3,4,9,10-bis(dicarboximide): The substituents in the amide nitrogens of perylene have almost no influence on the photophysical properties and are mainly introduced to increase the solubility of perylene diimides) (*25*).

All experiments support the proposed catalytic cycle shown in Fig. 4. Excited PDI* is reductively quenched by Et_3N to give $PDI^{\bullet-}$ and the radical cation of triethylamine ($Et_3N^{\bullet+}$) (*27*). Upon the second excitation, $PDI^{\bullet-*}$ reduces the substrate yielding the aryl radical precursor ($ArX^{\bullet-}$) and regenerating the neutral PDI. Fragmentation of $ArX^{\bullet-}$ yields the aryl radical, which abstracts a hydrogen atom from either $Et_3N^{\bullet+}$ or solvents to yield the reduction products, or reacts with unsaturated compounds yielding C–C coupling products. Gas chromatography–mass spectrometry (GC-MS) analysis of the crude product mixture confirmed the formation of diethylamine, and hydrogen atom abstraction reduction reactions in D_7-DMF gave deuterated products (see the supplementary materials).

Two conPET steps using perylene diimide dyes accumulate the energy from two visible light excitations. The process is a minimalistic chemical model of the Z scheme in biological photosynthesis and extends the scope of visible light photocatalysis to aryl chlorides. Highly reactive aryl radicals are obtained from stable, and in the case of aryl chlorides, inexpensive bulk chemicals, under very mild and metal-free reaction conditions.

REFERENCES AND NOTES

1. J. J. Concepcion, R. L. House, J. M. Papanikolas, T. J. Meyer, *Proc. Natl. Acad. Sci. U.S.A.* **109**, 15560–15564 (2012).
2. D. M. Schultz, T. P. Yoon, *Science* **343**, 1239176 (2014).
3. C. K. Prier, D. A. Rankic, D. W. C. MacMillan, *Chem. Rev.* **113**, 5322–5363 (2013).
4. J. Xuan, W. J. Xiao, *Angew. Chem. Int. Ed.* **51**, 6828–6838 (2012).
5. F. Teplý, *Collect. Czech. Chem. Commun.* **76**, 859–917 (2011).
6. D. P. Hari, P. Schroll, B. Koenig, *J. Am. Chem. Soc.* **134**, 2958–2961 (2012).
7. D. Ravelli, D. Dondi, M. Fagnoni, A. Albini, *Chem. Soc. Rev.* **38**, 1999–2011 (2009).
8. D. P. Hari, B. Koenig, *Angew. Chem. Int. Ed.* **52**, 4734–4743 (2013).
9. J. D. Nguyen, E. M. D'Amato, J. M. R. Narayanam, C. R. J. Stephenson, *Nat. Chem.* **4**, 854–859 (2012).
10. D. P. Hari, T. Hering, B. Koenig, *Angew. Chem. Int. Ed.* **53**, 725 (2014).
11. Y. X. Liu *et al.*, *Synlett* **24**, 507–513 (2013).
12. H. Kim, C. Lee, *Angew. Chem. Int. Ed.* **51**, 12303–12306 (2012).
13. The excited state redox potential of fac-Ir(ppy)3 is estimated to be −1.73 versus SCE (*9*). Some metal complexes with even stronger reducing power in the excited state have been reported but have not been applied to photoredox catalysis (*14*).
14. S. B. Harkins, J. C. Peters, *J. Am. Chem. Soc.* **127**, 2030–2031 (2005).
15. The Rehm-Weller equation estimates the reduction potential of a photoredox catalyst in its excited state from the ground-state redox potential and the $E_{0\text{-}0}$ transition energy (*28*).
16. For a recent example of two-step photoexcitation (Z scheme) of heterogeneous semiconductor in water splitting, see (*24*).
17. M. T. Pirnot, D. A. Rankic, D. B. C. Martin, D. W. C. MacMillan, *Science* **339**, 1593–1596 (2013).
18. L. Furst, B. S. Matsuura, J. M. R. Narayanam, J. W. Tucker, C. R. J. Stephenson, *Org. Lett.* **12**, 3104–3107 (2010).
19. J. M. R. Narayanam, J. W. Tucker, C. R. J. Stephenson, *J. Am. Chem. Soc.* **131**, 8756–8757 (2009).
20. D. A. Nicewicz, D. W. C. MacMillan, *Science* **322**, 77–80 (2008).
21. E. Cahard *et al.*, *Angew. Chem. Int. Ed.* **51**, 3673–3676 (2012).
22. C. Costentin, M. Robert, J. M. Savéant, *J. Am. Chem. Soc.* **126**, 16051–16057 (2004).
23. L. Pause, M. Robert, J. M. Saveant, *J. Am. Chem. Soc.* **121**, 7158–7159 (1999).
24. Y. Sasaki, H. Kato, A. Kudo, *J. Am. Chem. Soc.* **135**, 5441–5449 (2013).
25. F. Würthner, *Chem. Commun.* **2004** (14), 1564–1579 (2004).
26. D. Gosztola, M. P. Niemczyk, W. Svec, A. S. Lukas, M. R. Wasielewski, *J. Phys. Chem. A* **104**, 6545–6551 (2000).
27. M. J. Tauber, R. F. Kelley, J. M. Giaimo, B. Rybtchinski, M. R. Wasielewski, *J. Am. Chem. Soc.* **128**, 1782–1783 (2006).
28. D. Rehm, A. Weller, *Isr. J. Chem.* **8**, 259–271 (1970).
29. C. Ramanan, A. L. Smeigh, J. E. Anthony, T. J. Marks, M. R. Wasielewski, *J. Am. Chem. Soc.* **134**, 386–397 (2012).
30. M. E. Budén, J. F. Guastavino, R. A. Rossi, *Org. Lett.* **15**, 1174–1177 (2013).
31. Y. Cheng, X. Gu, P. Li, *Org. Lett.* **15**, 2664–2667 (2013).
32. R. A. Rossi, A. B. Pierini, A. B. Peñéñory, *Chem. Rev.* **103**, 71–168 (2003).
33. Z. Chami, M. Gareil, J. Pinson, J. M. Saveant, A. Thiebault, *J. Org. Chem.* **56**, 586–595 (1991).
34. M. Newcomb, in *Encyclopedia of Radicals in Chemistry, Biology and Materials*, C. S. Chatgilialoglu, A. Studer, Eds. (Wiley, Chichester, UK, 2012)pp. 107–124.
35. E. Shirman *et al.*, *J. Phys. Chem. B* **112**, 8855–8858 (2008).

ACKNOWLEDGMENTS

We thank the Deutsche Forschungsgemeinschaft (GRK 1626) for financial support. J.I.B. thanks the Alexander von Humboldt Foundation for a scholarship. We thank R. Vasold for his assistance in GC-MS measurements.

SUPPLEMENTARY MATERIALS

www.sciencemag.org/content/346/6210/725/suppl/DC1
Materials and Methods
Supplementary Text
Figs. S1 to S5
Table S1
References (*36*–*39*)

2 July 2014; accepted 1 October 2014
10.1126/science.1258232